Elaboration and properties of plasticised chitosan-based exfoliated nano-biocomposites

David Fengwei XIE [a,*], Verónica P. MARTINO [b], Parveen SANGWAN [c], Cameron WAY [c], Gregory A. CASH [d], Eric POLLET [b], Katherine M. DEAN [c], Peter J. HALLEY [a,d], Luc AVÉROUS [b,†]

[a] *Australian Institute for Bioengineering and Nanotechnology, The University of Queensland, Brisbane, Qld 4072, Australia*

[b] *BioTeam/ICPEES-ECPM, UMR 7515, Université de Strasbourg, 25 rue Becquerel, 67087 Strasbourg Cedex 2, France*

[c] *CSIRO Materials Science and Engineering, Gate 5 Normanby Rd, Clayton, Vic 3168, Australia*

[d] *School of Chemical Engineering, The University of Queensland, Brisbane, Qld 4072, Australia*

[*] Corresponding author. Tel.: +61 7 3346 3199; fax: +61 7 3346 3973.

Email addresses: f.xie@uq.edu.au; fwhsieh@gmail.com (D. F. Xie);

[†] Corresponding author. Tel.: +33 368852784; fax: +33 368852716.

Email addresses: luc.averous@unistra.fr (L. Avérous)

ABSTRACT

A series of plasticised chitosan-based materials and nanocomposites were successfully prepared by thermomechanical kneading. During the processing, the montmorillonite (MMT) platelets were fully delaminated. The nanoclay type and content and the preparation method were seen to have an impact on the crystallinity, morphology, glass transition temperature, and mechanical properties of the samples. When higher content (5%) of MMT–Na^+ or either content (2.5% or 5%) of chitosan-organomodified MMT (OMMT–Ch) was used, increases in crystallinity and glass transition temperature were observed. Compared to the neat chitosan, the plasticised chitosan-based nano-biocomposites showed drastically improved mechanical properties, which can be ascribed to the excellent dispersion and exfoliation of nanoclay and the strong affinity between the nanoclay and the chitosan matrix. The best mechanical properties obtained were Young's modulus of 164.3 MPa, tensile strength of 13.9 MPa, elongation at break of 62.1%, and energy at break of 0.671 MPa. While the degree of biodegradation was obviously increased by the presence of glycerol, a further increase might be observed especially by the addition of unmodified nanoclay. This could surprisingly contribute to full (100%) biodegradation after 160 days despite the well-known antimicrobial property of chitosan. The results in this study demonstrate the great potential of plasticised chitosan-based nano-biocomposites in applications such as e.g., biodegradable packaging materials.

Keywords:

Chitosan; Nano-biocomposite; Montmorillonite; Nanoclay; Biodegradation

1. Introduction

In the last years, polymers from renewable resources have attracted great attention due to their large availability, renewability, biocompatibility, and biodegradability (Yu, Dean, & Li, 2006). Among this group of polymers, chitosan, a linear polysaccharide consisting of (1,4)-linked 2-amino-deoxy-β-D-glucan, is a deacetylated derivative of chitin, which is the second most abundant polysaccharide found in nature after cellulose (Rinaudo, 2006). Chitosan has been found to be nontoxic, biodegradable, biofunctional, and biocompatible in addition to having antimicrobial characteristics, and thus has a great potential in packaging applications (Dutta, Tripathi, Mehrotra, & Dutta, 2009). These films have been reported to be able to form a barrier against moisture (Caner, Vergano, & Wiles, 1998), oxygen, and CO_2 (Hosokawa, Nishiyama, Yoshihara, & Kubo, 1990). The film properties depend on several parameters such as chitosan molecular weight and the degree of deacetylation, organic acid used, and the possible presence of plasticiser.

Recently, along with the exponential momentum of the development in polymer nanocomposites (Alexandre, & Dubois, 2000; Avérous, & Pollet, 2012; Bordes, Pollet, & Avérous, 2009; Pavlidou, & Papaspyrides, 2008; Sinha Ray, & Okamoto, 2003), much attention has been focused on the use of nano-sized fillers (at least one dimension in the nanometer range, i.e. 1–100 nm) in improving the performance of and adding new functionalities to polysaccharide-based materials. Chitosan-based nano-biocomposites have recently been reported with montmorillonite (MMT) (Depan, Kumar, & Singh, 2006; Depan, Kumar, & Singh, 2008; Wang et al., 2005b), carbon nanotubes (Lau, Cooney, & Atanassov, 2008; Wang, Shen, Zhang, & Tong, 2005a), metal oxide nanoparticles (Al-Sagheer, & Merchant, 2011; Kaushik et al., 2008; Khan et al., 2008; Li, Wu, & Zhitomirsky, 2010), cellulose nanofibres (Azeredo et al., 2010), nano-hydroxyapatite (Thein-Han, & Misra, 2009a, b) etc. as the reinforcements. These nanocomposites displayed improved properties such as

mechanical properties, thermal stability, moisture resistance and new properties such as electrical conductivity, and were aimed at various applications such as packaging, biosensors, tissue engineering (e.g., scaffolds) etc..

It is worth noting that, for preparing chitosan-based materials or nanocomposites, only solution casting or similar methods involving chemical reactions have been used in all the past studies. Solution casting is known to have the disadvantage in low efficiency and difficulty in scaling-up towards industrial applications. In addition, a great amount of environmentally unfriendly chemical solvents are used and released to the environment in this method. The reason for not using a melt processing method like extrusion or kneading in the past studies is that chitosan, like many other polysaccharides such as starch, has very low thermal stability and degrades prior to melting (infusibility). Therefore, even if the melt processing method is more convenient and highly preferred for industrial production, its adaptation for polysaccharide-based materials remains very difficult. While the processing issues of starch has been emphasised to some extent (Avérous, & Pollet, 2011; Chivrac, Pollet, & Avérous, 2009; Li et al., 2011; Liu, Xie, Yu, Chen, & Li, 2009; Xie, Halley, & Avérous, 2012), there has been very limited focus on the melt processing of chitosan-based materials/nanocomposites.

In the current study, we aim to develop a new method by melt processing to fabricate plasticised chitosan-based nano-biocomposites. Our recent study (Epure, Griffon, Pollet, & Avérous, 2011) has demonstrated the successful use of an innovative melt processing method (internal mixer) as an alternative route to solution casting, for preparing plasticised chitosan-based materials. This current work followed the same processing protocol but focused on the development of chitosan-based nano-biocomposites. Montmorillonite (MMT), which possesses some strong advantages such as wide availability, low cost, versatility, eco-friendliness, and low toxicity and has been frequently used in other polymer nanocomposite

systems (Alexandre, & Dubois, 2000; Avérous, & Pollet, 2012; Bordes et al., 2009; Pavlidou, & Papaspyrides, 2008; Sinha Ray, & Okamoto, 2003), will be used as the nanofiller. The effects of nanoclay content, organomodification, preparation method on the structure, properties, and biodegradation of the plasticised chitosan-based nano-biocomposites were examined.

2. Materials and methods

2.1. Materials

Two types of chitosan were used in the experimental work and their characteristics are shown in Table 1. ChitoClear™ was provided as a white powder with particle diameter lower than 1 mm (100% through mesh 18). The original moisture content of ChitoClear was 8.7 wt.% (wet basis). KiOnutrime-Cs® was provided as a powder in sandy brown colour and in even finer particle size. The original moisture content of KiOnutrime-Cs was 8.3% (wet basis). Considering the difference in molecular chain length, ChitoClear was used as the matrix of the chitosan-based nano-biocomposites, while KiOnutrime-Cs was used as the organomodifier for the nanoclay. The Dellite® LVF sodium montmorillonite (MMT–Na^+) was supplied by Laviosa Chimica Mineraria S.p.A. (Italy) and has a cationic exchange capacity (CEC) of 1050 μequiv/g. Glycerol (99.5% purity, from Novance, France), acetic acid (Fluka, Sigma-Aldrich), and sodium hydroxide (Carlo Erba Réactifs – SdS, France), and sodium bromide (Sigma-Aldrich) were used as received. Deionised water was used for the sample preparation.

Table 1 Two chitosans used in the experimental work (the data are provided by the suppliers).

Commercial name	KiOnutrime-Cs®	ChitoClear™

Supplier	KitoZyme	Primex
Source	Aspergillus niger (mushroom)	Pandalus borealis (shrimp)
Molecular mass	1.5×10^7 Da	$2.5 \times 10^8 - 3.0 \times 10^8$ Da
Deacetylation degree	78–80%	96%

114

115 *2.2. Sample preparation*

116 *2.2.1. Organomodification of montmorillonite*

117 Chitosan solution was prepared by adding 4.754 g (dry basis) of the KiOnutrime-Cs
118 Chitosan to 500 mL of 1% (v/v) acetic acid (AcOH). The solution was stirred at room
119 temperature overnight. The pH of the solution was then adjusted to 4.9 with NaOH solution.
120 In parallel, a stock of well-dispersed clay suspension was prepared by adding 20 g of MMT–
121 Na^+ into 500 mL of water and treating with sonication at 60 °C for 4 h. Then, the chitosan
122 solution and the MMT–Na^+ suspension were mixed together and the mixture was stirred at
123 60 °C for 24 h. The mixture was centrifuged at 3000 rpm for 15 min, and then the
124 supernatants were discarded. The precipitate was washed with distilled water and centrifuged
125 again at the same condition, which was repeated twice to make it free from acetate. Hence,
126 the final paste of chitosan-organomodified MMT (OMMT–Ch) was obtained with moisture
127 content of 94.6%. Part of the paste was oven-dried (50 °C, overnight) into powder for use
128 later. Here, the mass ratio of chitosan and clay were thus determined to achieve a monolayer
129 of chitosan absorbed into the nanoclay interlayer spacing through a cationic procedure with
130 respect to the CEC of the nanoclay (Darder, Colilla, & Ruiz-Hitzky, 2003).

131

132 *2.2.2. Preparation of chitosan-based nanocomposites*

133 The preparation procedure for the chitosan-based nanocomposites used here was similar
134 to that in our previous work (Epure et al., 2011), with modifications especially regarding the

addition of nanoclay. Seven samples with different formulation and/or preparation method were prepared, with the details and the sample codes listed in Table 2. As a typical procedure, glycerol was first introduced into the chitosan powder and manually mixed, followed by the addition of nanoclay (in the form of either paste or dried powder) with further manual mixing. Then, acetic acid aqueous solution (3%, v/v) was added dropwise to the chitosan–glycerol–nanoclay mixture with continuous manual mixing to obtain a paste with a final chitosan concentration of 25 wt.%. In some formulations where no glycerol or clay was used, the above procedure was accordingly adjusted. Also the amounts of the added 3% acetic acid solution listed in Table 2 were adjusted by taking into account the moisture content with the OMMT–Ch paste. However, this would hardly vary the effect of acetic acid solution because the pH value just changes from 2.53 to 2.68 even when the concentration of acetic acid varies from 3.0% to 1.5% (v/v).

Table 2 Formulations of the chitosan-based materials/nanocomposites [a].

Sample code	Chitosan [b]	Glycerol	3% AcOH solution [c]	MMT	OMMT–Ch [d]
G0	100	0	300	–	–
G10	90	10	270	–	–
G25	75	25	225	–	–
G25M2.5	75	25	225	2.5	–
G25M5.0	75	25	225	5.0	–
G25O2.5p	75	25	225 (167.7)	–	2.5 (paste)
G25O5.0p	75	25	225 (110.4)	–	5.0 (paste)
G25O2.5d	75	25	225	–	2.5 (dried)
G25O5.0d	75	25	225	–	5.0 (dried)

[a] The numbers stand for the portions in weight; [b] Listed are the values of dry chitosan; [c] The numbers in brackets indicate the actual additions after subtracting the water content in the OMMT–Ch paste; [d] Listed are the values of the corresponding inorganic part (MMT) of OMMT–Ch.

The mixtures with different formulations obtained above were then thermo-mechanically kneaded in a Haake Rheocord 9000 internal batch mixer with twin roller rotors at 80 °C for 15 min, with a rotor speed of 100 rpm. Finally, the resulting materials were compression moulded at 110 °C temperature and 160 bar pressure for 15 min (with a venting process after 8 min), immediately following by cooling at room temperature for 5 min. After compression moulding, the chitosan sheets of 2 mm thickness were obtained.

The sheets were then conditioned in desiccators at 57% relative humidity (achieved with saturated NaBr solution) and ambient temperature. Toluene was also placed in desiccators for preventing the growth of microorganisms in the samples. The samples were thus conditioned for one month before any characterisation work.

2.3. Characterisation

2.3.1. X-ray diffraction analysis

X-ray diffraction (XRD) was performed on the chitosan sheets after conditioning. XRD patterns were obtained at room temperature on a powder diffractometer Siemens D5000 (Germany). Cu Kα radiation (λ = 1.5406 Å) at 35 kV and 25 mA was used. Both small-angle and wide-angle tests were carried out for each formulation. In small-angle tests, the scattering range was 2θ = 1.5–9° by step size of 0.01 and a scanning speed of 4 sec/step. The clay inter-layer spacing (also called *d*-spacing) values (d_{001}) were calculated from the nanoclay diffraction peak using the Bragg's law:

$$2d_{001}\sin\theta = n\lambda \qquad (1)$$

where, d_{001} is the spacing between the planes in the atomic lattice, θ is the angle between the X-ray ray and the scattering planes, n is an integer, and λ is the wavelength of X-ray wave. In wide-angle tests, a range of $2\theta = 8–30°$ by step size of 0.02° per 3 sec was used.

2.3.2. Transmission electron microscopy

Samples for microscopy were embedded in epoxy resin which was cured for 2 days at 60 °C. Sections 60–70nm thick were cut from the blocks on a Leica M80 Ultra Microtome using a diamond knife. The sections were transferred onto 400 mesh copper grids which were stained with a 0.1% aqueous solution of RuO_4 for 5 min. TEM images were obtained using a JEOL 1010 transmission electron microscope at 100kV using spot size 6.

2.3.3. Dynamic mechanical thermal analysis

Dynamic mechanical thermal analysis (DMTA) was performed on rectangular tensile bars of the conditioned plasticised chitosan samples by using a Rheometric Scientific™ DMTA IV machine with dual cantilever bending mode from −100 to 110 °C, with a heating rate of 1.5 °C/min, a frequency of 1 Hz, and a strain value of 0.05%. The dynamic storage modulus (E'), loss modulus (E''), and loss tangent ($\tan \delta = E''/E'$) were obtained from the tests. To prevent water evaporation during the tests, the specimens were coated with Vaseline grease. No swelling of the specimens was observed, suggesting no adverse effect of Vaseline.

2.3.4. Thermogravimetric analysis

Thermogravimetric analyses (TGA) were performed on a SDT Q600 apparatus from TA Instruments (USA). The analyses were carried out under either air or helium environment. The samples (ca. 3 mg placed in a platinum pan) were heated from 20 to 700 °C at 10 °C/min.

198 The degradation temperature was determined from the peak temperature of the derivative
199 weight loss curve.
200
201 *2.3.5. Tensile tests*
202 Tensile tests were performed with an MTS® 2/M universal testing machine on dumbbell-
203 shaped bars cut from the sheets with a constant deformation rate of 5 mm/min. The testing
204 section of the bar was 30 mm in length and 5 mm in width. The testing temperature was
205 maintained at 23 °C with an environment chamber used with the testing machine. Young's
206 modulus (E), tensile strength (σ), elongation at break (ε_b), and energy at break (U_b) were
207 determined from 7 specimens for each chitosan sample.
208
209 *2.3.6. Compost characterisation*
210 Approximately 2–3 month mature compost samples were collected from a commercial
211 composting facility (Natural Recovery Systems, Victoria, Australia) and sieved through a
212 sterile brass sieve (8-mm aperture size). To determine the dry weight of the compost, 25 g of
213 the fresh compost sample was weighed in an analytical balance and placed in a hot air oven at
214 105 °C for 3–5 days or until constant weight. The conversion factor of fresh to dry weight for
215 the compost was calculated, and the results were expressed per gram (dry weight) of the
216 compost. The pH of the compost was determined by mixing the compost in deionised water
217 (ratio 1:5). Volatile solids were calculated by subtracting the residue (left after incineration at
218 550 °C) from total dry solids of the same sample. Volatile solids were expressed as per gram
219 (dry weight) of the compost. Total organic carbon and total nitrogen were determined by
220 HRL Technology (Mulgrave, Victoria, Australia) using the methods APHA 5310B and
221 APHA 4500 TKN respectively. The compost characteristics were pH 7.5, dry weight 52%,
222 volatile solids 44% (dry weight), and C/N ratio 10 (on oven-dried basis).

223

224 *2.3.7. Biodegradation tests*

225 The biodegradability of the chitosan samples was determined according to the Australian
226 Standard AS ISO 14855. The test material was reduced in size to achieve maximum surface
227 area of each individual piece of the test material, approximately 2 cm × 2 cm. Each
228 composting vessel contained 100 g of the test material and 600 g of the compost inoculum,
229 both on dry weight basis. Each material was tested in triplicate including the blank (the
230 compost only) and positive (a mixture of cellulose and the compost) references. All
231 composting vessels were then placed inside an in-house built respirometer unit (Way, Wu,
232 Dean, & Palombo, 2010) and the temperature was maintained at 58±2 °C for a period of 160
233 days. During this degradation period, the compost moisture content was maintained at 48–
234 50% and the pH at 7.8–8.5 to ensure favourable conditions for the compost microorganisms
235 involved in the biodegradation process. Aerobic conditions were maintained by continuous
236 supply of sufficient airflow to the bioreactors and the contents of each of the bioreactors were
237 mixed once a week to ensure uniform distribution of air throughout the compost. The evolved
238 CO_2 and flow rate data were continually data-logged by computer for each respective
239 bioreactor. The theoretical amount of CO_2 produced by the test and reference materials was
240 assessed and the degree of biodegradation, D_t, was calculated (for the test and reference
241 materials) using following equation, as described in the Australian Standard AS ISO 14855:

242 $$D_t = \frac{(CO_2)_T - (CO_2)_B}{THCO_2} x100 \qquad (2)$$

243 where $(CO_2)_T$ is the cumulative amount of carbon dioxide evolved in each bioreactor
244 containing the test material (in grams per bioreactor), and $(CO_2)_B$ is the mean cumulative
245 amount of carbon dioxide evolved in the blank vessel (in grams per bioreactor)

246

3. Results and discussion

3.1. Nanostructure and morphology

Figure 1 shows the XRD patterns of MMT–Na^+, OMMT–Ch, and the different chitosan samples after conditioning. From Figure 1a, it can be seen that MMT had a sharp peak at 2θ of 7.18°, which corresponds to the original d_{001} of 12.3 Å. After organomodification with chitosan, this peak disappeared and only a slight shoulder appeared at 2θ of around 4.48°, which corresponds to a d_{001} of 19.7 Å. According to Darder et al. (2003), this d_{001} value demonstrates the uptake of at least one chitosan layer by the clay. This indicates that the chitosan with relative smaller molecular mass (KiOnutrime-Cs) had been successfully intercalated into the interlayer spaces of MMT–Na^+. From Figure 1b, it is interesting to see that there was no sharp peak for all the samples. Even G25M2.5 and G25M5.0 only showed a very slight peak at 2θ of around 3.96°, corresponding to a d_{001} of 22.3 Å. It could be that the intensive thermomechanical treatment during processing induced the intercalation of the matrix chitosan (ChitoClear) into the interlayer spaces of MMT–Na^+, thus well dispersing the nanoclay. Overall, irrespective of the formulation and preparation method, the nanoclay was well dispersed into the plasticised chitosan matrix, forming exfoliated nanocomposites.

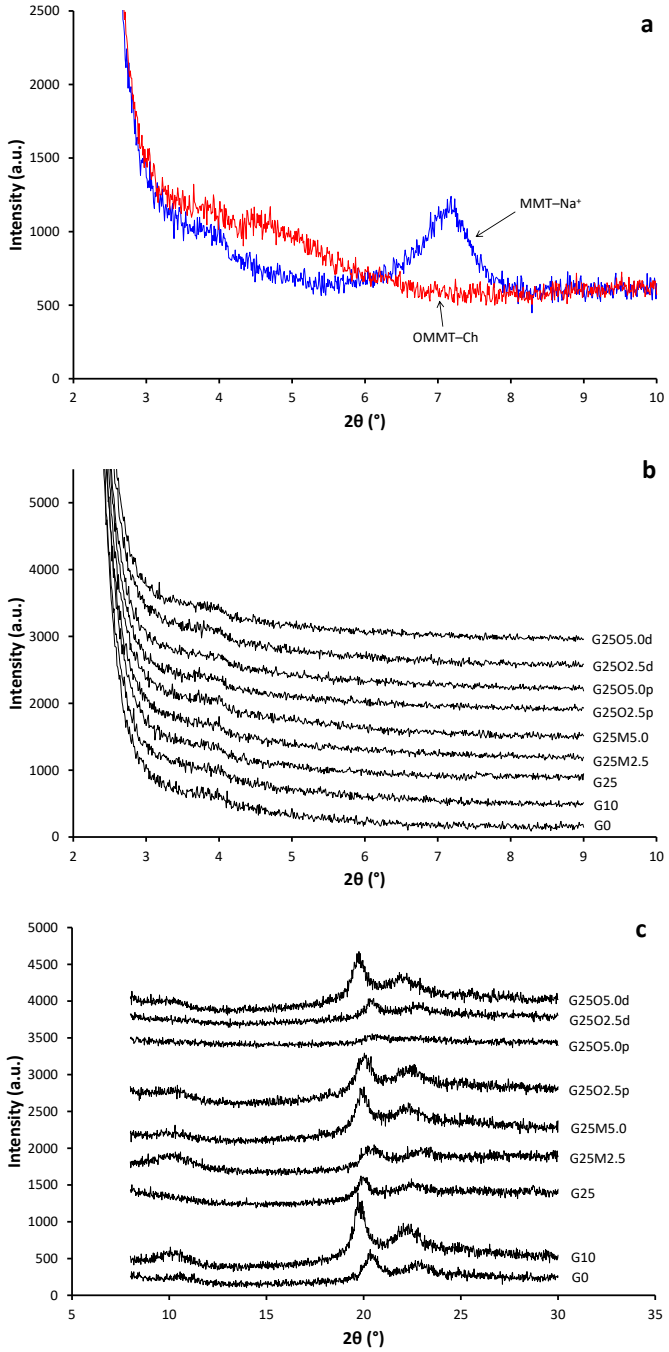

Figure 1 XRD results of both MMT–Na^+ and OMMT–Ch in small angle range (1.5–9°) (a), the different chitosan samples in small angle range (1.5–9°) (b), and the different chitosan samples in wide angle range (8–30°) (c).

In order to confirm to the dispersion of nanoclay in the samples and also to give definitive conclusions about the defined structure, TEM was also carried out and the morphological

results are shown in Figure 2. It can be seen from Figure 2 that, while G25M5.0, G25O5.0p, and G25O5.0d all showed good dispersion of the nanoclay, the morphological patterns of these samples were completely different. As far as non-modified clay was concerned, G25M5.0 showed an exfoliated morphology containing individually separated silicate layers, which was similar to the results reported before (Wang et al., 2005b). However, some clay stacks could also exist, which might correspond to the slight peak in XRD. When OMMT–Ch was used as a paste, G25O5.0p displayed a well exfoliated structure but corrugations were also shown along with the silicate layers. This corrugation pattern has also been observed before by Darder et al. (2003) for the nanocomposites resulting from the intercalation of chitosan into MMT through a cationic exchange process, and is indicative of the constrained action of the chitosan organomodifier interacting with the nanoclay substrate. In contrast, if OMMT–Ch was added after drying, a well exfoliated morphology was obtained which no longer displayed corrugation but showing instead a more flocculated or cloud-like pattern. This could be due to the edge-edge interaction of the OMMT–Ch silicate layers (Sinha Ray, Okamoto, & Okamoto, 2003). After drying, the silicate layers might come closer with the chitosan organomodifier, which, together with the water molecules removal, may lead to enhanced interactions between silicate layer surfaces and the chitosan organomodifier, resulting in some stacking of silicate layers as observed on the G25O5.0d TEM pictures. In spite of the delamination by the thermo-mechanical process, the edge-edge interaction of the silicate layers could remain forming the flocculated morphology.

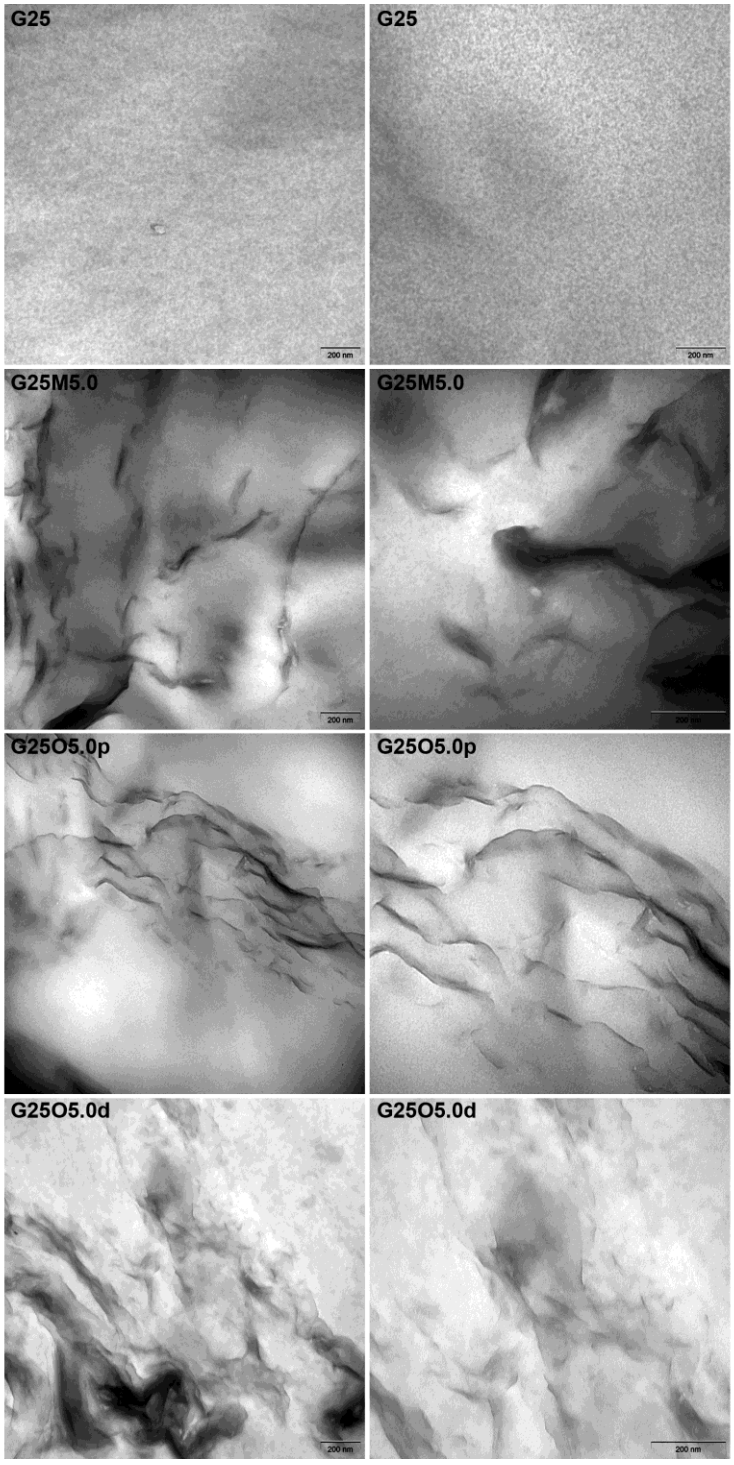

Figure 2 TEM images of the different chitosan samples.

3.2. Crystalline structure

The crystalline structure of the different chitosan samples can be described from the wide-angle XRD results in Figure 1c. Typically, there are three main peaks at around 10°, 20°

and 22°. The peak at 10° (020 reflection) is assigned to the hydrated crystals due to the integration of water molecules in the crystal lattice and the peaks located at 20° (100 reflection) and 22° (110 reflection) are attributed to the regular crystal lattice of chitosan (Kittur, Vishu Kumar, & Tharanathan, 2003). The intensities of these peaks are much inferior to those of raw chitosan which displays a very high crystallinity (ca. > 80%) (Epure et al., 2011). This is not unexpected since processing could destroy the crystalline structure of chitosan, which has also been observed in other studies (Epure et al., 2011; Kittur et al., 2003). Besides, it can be observed that there are some differences in these peaks among the different samples. Particularly, G10 displayed a relatively higher crystallinity. This sample might have a right amount of glycerol, facilitating recrystallisation. However, when the glycerol content was even higher (25%), a large amount of glycerol exists between the chitosan molecules, making the recrystallisation less easy, as evidenced by the XRD result of G25. With the addition of nanoclay (either MMT–Na^+ or OMMT–Ch), the intensities of the peaks at 20° and 22° generally became larger (except for G25O2.5p), indicating that the existence of nanoclay facilitated the chitosan recrystallisation. The XRD pattern of G25O5.0p was largely compressed, indicating a more amorphous structure. This can be possibly explained by the less chance for the chitosan to interact with the nanoclay which was initially bound with water and thus recrystallisation being less significant.

3.3. DMTA results

Considering the semi-crystalline structure of the chitosan samples after processing and conditioning, DMTA was also carried out to investigate the relaxation temperatures. Figure 3 shows the typical results from the DMTA study. It can be seen that two peaks are easily identified for the samples. Previous studies have generally shown that the peak at higher temperature is related to α relaxation, which could be linked to the glass transition of the

chitosan, and the one at lower temperature corresponds to the secondary relaxation (β relaxation) of the plasticiser-rich domains (Quijada-Garrido, Laterza, Mazón-Arechederra, & Barrales-Rienda, 2006; Quijada-Garrido, Iglesias-González, Mazón-Arechederra, & Barrales-Rienda, 2007). However, the current work shows that the two peaks appear even without glycerol. Thus, the peak at lower temperature could be more appropriately attributed to the motions of the side chains or lateral groups of chitosan interacting with small molecules of water and/or glycerol by hydrogen bonding. In addition, for some of the samples especially G0, there is another peak/shoulder at even higher temperature (ca. 80 °C). This peak has also been observed by Quijada-Garrido et al. (2006) and has been attributed to the transformation of chitosonium acetate units formed during the sample preparation.

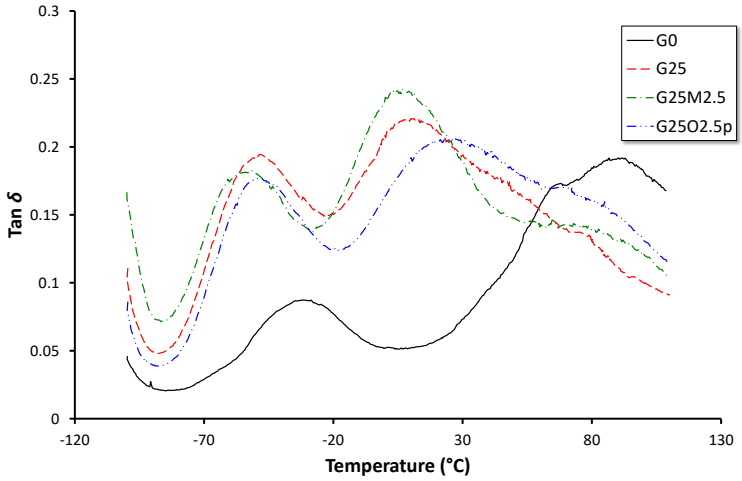

Figure 3 DMTA results of the different chitosan samples.

The maxima (T_β and T_α) that correspond to the β- and α-processes (respectively) obtained from DMTA curves of all the samples are given in Table 3. The results show that an increase in glycerol content from nil to 25% decreased both the T_α and T_β, indicating an increase in molecular mobility of the chitosan samples. Surprisingly, the addition of 2.5% of MMT–Na^+ (G25M2.5) further decreased these two temperatures. One possible reason could be that the

distribution of MMT–Na^+ allows more homogeneous distribution of water and glycerol across the system, resulting in better plasticisation effect. Interestingly, higher amounts (5%) of MMT (G25M5.0) showed slightly higher values of both T_α and T_β compared with those of G25M2.5, indicating an extra restriction effect on the movement of the chitosan molecules. When OMMT–Ch, which may have better affinity with the chitosan matrix due to its organomodification than MMT–Na^+, was used, G25O2.5p, G25O5.0p, G25O2.5d, and G25O5.0d showed increased T_α and T_β values, with the increase in T_α more significant. Furthermore, it is noticed that the T_α values of G25O5.0d was higher than that of G25O5.0p, indicating that the addition of the nanoclay in dry form allowed a greater chance to interact with the chitosan and thus a greater restriction effect. However, this was not case when the loading level was lower (the T_α values of G25O2.5d was lower than that of G25O2.5p), because the restriction effect might not be strong enough at this content level while water still mostly interacted with the chitosan.

Table 3 Relaxation temperatures (T_α and T_β, obtained from tan δ curves), thermal decomposition temperatures ($T_{d,\,air}$ and $T_{d,\,He}$, obtained from derivative weight loss curves), and degree of biodegradation (DB) after 160 days (with cellulose for comparison purposes), of plasticised chitosan-based materials/nanocomposites after conditioning.

Sample	T_β (°C)	T_α (°C)	$T_{d,\,air}$ (°C)	$T_{d,\,He}$ (°C)	DB (%)[a]
G0	−31	67.8	302.5	307.7	64
G10	−44.4	41.4	305.0	312.8	95
G25	−48.5	10.5	302.9	308.3	98
G25M2.5	−54.1	4.5	300.3	300.8	101
G25M5.0	−52.4	6.7	296.7	307.2	105

G25O2.5p	−49.5	23.3	300.1	307.3	100
G25O5.0p	−52.3	23.6	297.1	304.0	95
G25O2.5d	−50.0	19.5	302.4	305.7	–
G25O5.0d	−50.7	24.6	302.2	305.8	–
Cellulose	–	–	–	–	90

[a] Co-variance of biodegradation values at the end of testing was up to ± 7%.

3.4. Thermal stability

In order to investigate the thermal stability of the different samples, TGA experiments were carried under either air or helium environment, and the results of derivative weight loss are shown in Figure 4. From this figure, three thermal decomposition peaks can be easily identified when air was used as the environmental gas; however, only the first two peaks are observed if helium gas was used. According to the previous study (Wang et al., 2005b), the first peak before 200 °C was mainly due to the evaporation of water; the peak ranged from 200 °C to 450 °C could be ascribed to both the evaporation of glycerol and the thermal decomposition and deacetylation of chitosan; and the third peak ranged from 450 °C to 700 ° at even higher temperature (only under air environment) might be assigned to the oxidative degradation of the carbonaceous residue formed during the second step.

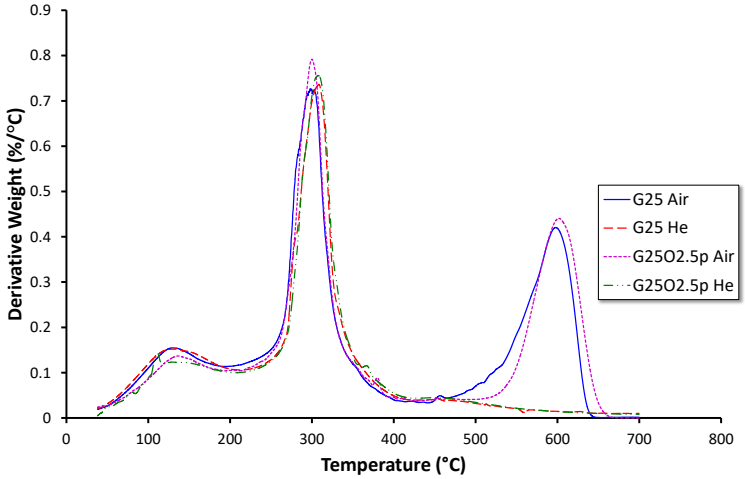

Figure 4 TGA results of the different chitosan samples.

The thermal decomposition temperatures (the second step) (at maximum decomposition rate) of chitosan under air ($T_{d,\,air}$) or helium ($T_{d,\,He}$) environment for all the samples are listed in Table 3. It can be seen that the $T_{d,\,He}$ is generally higher than the $T_{d,\,air}$ for each sample. This is reasonable considering that the oxygen in the air could accelerate the thermal decomposition of chitosan. It can also be observed that the addition of the nanoclay did not show a positive impact on the thermal stability of the materials, irrespective of the preparation method, the type of nanoclay, and the addition content. The hydrophilic groups of MMT could even deteriorate the thermal stability of the plasticised chitosan-based materials especially under air environment, as evidenced by the $T_{d,\,air}$ values of G25M5.0 and G25O5.0p. Of course, the thermal decomposition results could also be related to the crystallinity of the materials. As shown in Table 3, the higher $T_{d,\,air}$ and $T_{d,\,He}$ of G10 could be ascribed to its higher crystallinity as observed from the XRD results.

3.5. Mechanical properties

From Figure 5a and b, the formulation and preparation method influenced the E and σ in a similar way, with the only exception of G25O5.0p. The mechanical properties of the unfilled

394 samples (G0, G10, and G25) were quite low. With higher glycerol content, the *E* and σ were
395 reduced to lower values, which is as expected and is similar to the results in our previous
396 study (Epure et al., 2011). Although the addition of 2.5% of MMT–Na^+ (G25M2.5) showed
397 little improvement (which can be attributed to the low crystallinity and the facilitation of
398 plasticisation as discussed before), higher amounts of MMT–Na^+ or the addition of OMMT–
399 Ch generate increased *E* and σ. Comparing with the neat matrix (G25) which had a *E* of
400 11.1 MPa and a σ of 2.4 MPa, the values of G25O5.0d were significantly increased to
401 100.4 MPa and 13.9 MPa, respectively. This can be attributed to the homogeneous dispersion
402 of the nanoclay as well as the favourite interaction between the organomodified nanoclay and
403 the chitosan matrix. Besides, addition of dried OMMT–Ch powder at 2.5% loading level
404 could generate higher values of both *E* and σ than addition of the OMMT–Ch paste at the
405 same loading level. Again, this could be due to a greater chance for the nanoclay to interact
406 with the chitosan when it was not initially bound with water. However, it is interesting to
407 observe that G25O5.0p showed the highest *E* among all the samples, but a lower σ comparing
408 to other OMMT–Ch filled samples. The low σ could be ascribed to the low crystallinity,
409 although the reinforcing effect of the nanoclay still contributed to the dramatically increased
410 stiffness.
411

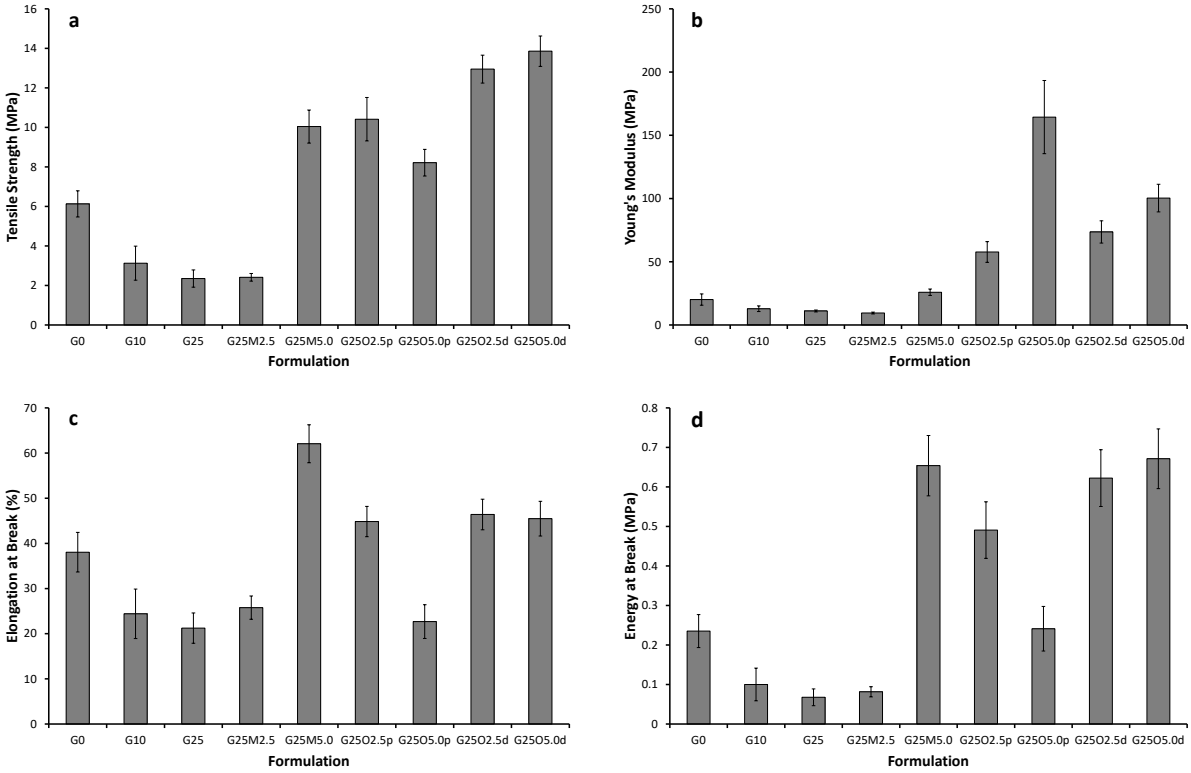

412

413 Figure 5 Young's modulus (a), tensile strength (b), elongation at break (c), and energy at
414 break (d) values of the different chitosan samples. The error bars stand for the
415 standard deviations.

416

417 It can be seen from Figure 5c and d that the formulation and preparation method affected
418 the ε_b and the U_b in a similar way as well. As that of E and σ, the pattern of change in ε_b and
419 U_b among G0, G10, and G25 can be related to the plasticisation by glycerol. When the
420 nanofiller was incorporated, it is quite interesting to note that the ε_b and U_b were not reduced
421 (even though the reverse trend normally is observed for a wide range of polymer
422 nanocomposites). This is especially the case when higher content (5%) of MMT–Na^+ was
423 used and/or addition of dried nanofiller was used. G25M5.0 displayed the highest ε_b (62.1%),
424 which was twice higher than that (21.2%) of its neat matrix (G25). Besides, addition of 5% of
425 MMT–Na^+/OMMT–Ch drastically increased the U_b from 0.068 MPa of G25 to 0.654 of
426 G25M5.0 and to 0.671 MPa of G25O5.0d. Again, this can be attributed to the better

reinforcing effect at higher nanoclay addition level and the better interaction between the nanoclay and chitosan when the nanoclay was added in dry form. When the paste of OMMT–Ch was added, the reinforcing effect of the nanofiller became less significant due to a less chance for the nanoclay to interact with the chitosan which was bound with water. Consequently, G25O2.5p and G25O5.0p (especially the latter) showed reduced ε_b and U_b values than G25O2.5d and G25O5.0d.

3.6. Biodegradation

The cumulative CO_2 and percentage biodegradation profiles for each test sample are shown in Figure 6a and b respectively. Steady rates of carbon dioxide evolution from each composting vessel indicate that test materials were actively metabolised by microbial population present in the compost (Figure 6a). Similar results were observed by Xu, McCarthy, Gross, & Kaplan (1996) during their biodegradation studies on acetylated chitosan films. It was observed that the biodegradation of the plasticised chitosan samples, with or without the addition of nanoclay (i.e. G10, G25, G25M2.5, G25M5.0, G25O2.5p, and G25O5.0p) was initiated immediately after incubation in compost, without any lag phase, whereas the unplasticised chitosan (G0) degraded relatively much slower (Figure 6b). All plasticised samples achieved more than 50% biodegradation within the first two weeks of composting. In comparison, G0 had an initial lag phase (~3 days) and it reached approximately 18% biodegradation at the end of second week. The increased susceptibility of the plasticised chitosan to biodegradation was probably due to the presence of glycerol. During week 3, a significant drop in degree of biodegradation was observed for all the chitosan samples (but not in the positive reference, cellulose). Previous studies have reported that alkyl amides and their corresponding *N*-derivatives alkyl amines have antimicrobial properties (Kabara, Conley, & Truant, 1972). Chitosan, a deacetylated form of chitin, is a

polymer with repeating units of disaccharides having amino groups (1,4)-2-amino-2-deoxy, β-D-glucan, and it is reported to have antibacterial effect (Guo et al., 2006; Kean, & Thanou, 2010). The degradation mechanism of chitosan in compost is not clearly understood. Therefore, we hypothesise that, in the composting vessels containing the chitosan samples, microbial activity was significantly influenced in the presence of certain inhibitory substances produced as a by-product during the chitosan biodegradation (Badawy, & Rabea, 2011; Tikhonov et al., 2006). As a result, the amount of CO_2 produced in the bioreactors containing the chitosan samples was dramatically reduced as compared to the blank compost, resulting in the significantly reduced biodegradation values. As time progressed (i.e. during week 4), the inhibitory substances were presumably further degraded into products which were less effective in inhibiting microbial activity, or easily susceptible to microbial degradation. As a result, a steady rate of biodegradation was observed for all test samples until week 8. After 2 months of composting, G0 achieved 45% biodegradation whereas the plasticised chitosan samples biodegraded by 60–80%. During week 9, a slight decrease in the level of biodegradation was observed for all the chitosan samples but not as significant as observed during week 3. It is likely that this slight decrease was caused by a similar mechanism (as seen in week 3), but less severe due to a further decrease in the chain-length in the degradation by-products. A steady progress of biodegradation was observed thereafter. The overall degree of biodegradation of the samples G25M2.5, G25M5.0, G25O2.5p, and G25O5.0p did not seem to be dramatically affected by addition of nanoclay (Table 3) as shown in Figure 6b. Exfoliated clay creates torturous path for oxygen permeation and water absorption thus should influence the rate of biodegradation. In the present study, the samples containing the modified nanoclay (G25O2.5p and G25O5.0p) demonstrated no such effect on biodegradation due to the sample thickness and high surface area for microbial attack. The unmodified nanoclay samples (G25M2.5 and G25M5.0) showed a slight increase in their

relative degree of biodegradation (relative to G25) due to the inherent defects in the samples by MMT–Na^+. Interestingly, despite the antimicrobial nature of chitosan, 100% biodegradation was achieved for G25M2.5, G25M5.0, and G25O2.5p after 160 days of composting. More than 100% biodegradation observed for samples G25M 2.5 and G25M5.0 was probably due to an increased rate of respiration of microorganisms metabolising the available test material i.e. carbon-source (Funabashi, Ninomiya, & Kunioka, 2009). Nevertheless, the detailed biodegradation mechanism of chitosan and plasticised chitosan-based nanocomposites needs further investigation.

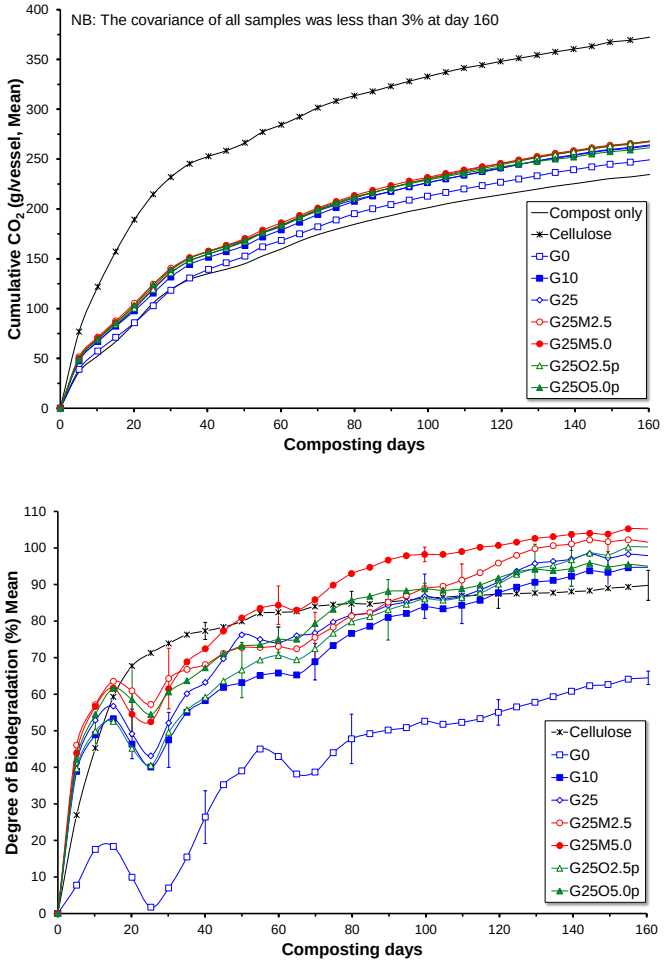

Figure 6 The cumulative CO_2 data (a) and the degrees of biodegradation (b) as a function of composting time for cellulose and the different chitosan samples.

4. Conclusion

In this study, a novel processing method has been developed in the preparation of chitosan-based nano-biocomposites. Comparing to a typical solution casting method which has been used in many other studies of chitosan-based materials, this process demonstrates the high efficiency and great ability in well dispersing the nanoclay into the chitosan matrix. The XRD and TEM results showed that MMT could be largely exfoliated in the chitosan matrix during thermal kneading, no matter organomodification of MMT with chitosan was carried out.

Nevertheless, the formulation and preparation method could have an impact on the characteristics of the samples, such as crystallinity and glass transition temperature. Particularly, the addition of 2.5% MMT–Na^+ might result in greater distribution of glycerol and water and thus better plasticisation. In contrast, when higher content (5%) of MMT–Na^+ was added or either content (2.5% and 5%) of OMMT–Ch was used, increases in crystallinity and glass transition temperature were observed. When OMMT–Ch was added in paste form, which means the nanoclay was initially bound with water, the interaction between the nanoclay and chitosan could be weaker and thus a less reinforcing effect of the nanoclay was shown. In contrast, addition of dry OMMT–Ch resulted in a better interaction of the nanofiller with the chitosan matrix. The plasticised chitosan-based nanocomposites showed obviously improved E, σ, ε_b, and U_b. The best mechanical properties obtained were E of 164.3 MPa, σ of 13.9 MPa, ε_b of 62.1%, and U_b of 0.671 MPa. This can be ascribed to the excellent dispersion of nanoclay and strong affinity between the nanoclay and the chitosan matrix. Nevertheless, the highest performance in different mechanical properties could be different regarding the formulation and preparation method. While the degree of biodegradation was obviously increased by the addition of glycerol, a marginal increase was observed by the further addition of the unmodified nanoclay. This led to complete

514 biodegradation after 160 days despite the well-known antimicrobial property of chitosan.
515 Consequently, this study demonstrates the great potential of plasticised chitosan-based nano-
516 biocomposites in applications such as biodegradable packaging.
517
518 **Acknowledgements**
519 Dr. D. F. Xie acknowledges the funds provided by the "Australian Academy of Science
520 Scientific Visits to Europe 2010–2011" and "The University of Queensland Travel Award for
521 International Collaborative Research 2011 (Category 2)" programs for his visits to Université
522 de Strasbourg, France for the collaborative research work. The authors acknowledge the
523 facilities, and the scientific and technical assistance, of the Australian Microscopy &
524 Microanalysis Research Facility at the Centre for Microscopy and Microanalysis, The
525 University of Queensland.
526
527

References

Al-Sagheer, F. A., & Merchant, S. (2011). Visco-elastic properties of chitosan–titania nano-composites. *Carbohydrate Polymers, 85*(2), 356-362.

Alexandre, M., & Dubois, P. (2000). Polymer-layered silicate nanocomposites: preparation, properties and uses of a new class of materials. *Materials Science and Engineering: R: Reports, 28*(1-2), 1-63.

Avérous, L., & Pollet, E. (2011). Biorenewable nanocomposites. *MRS Bulletin, 36*(09), 703-710.

Avérous, L., & Pollet, E. (2012). *Environmental Silicate Nano-Biocomposites*. London: Springer-Verlag.

Azeredo, H. M. C., Mattoso, L. H. C., Avena-Bustillos, R. J., Filho, G. C., Munford, M. L., Wood, D., & McHugh, T. H. (2010). Nanocellulose Reinforced Chitosan Composite Films as Affected by Nanofiller Loading and Plasticizer Content. *Journal of Food Science, 75*(1), N1-N7.

Badawy, M. E. I., & Rabea, E. I. (2011). A Biopolymer Chitosan and Its Derivatives as Promising Antimicrobial Agents against Plant Pathogens and Their Applications in Crop Protection. *International Journal of Carbohydrate Chemistry, 2011*.

Bordes, P., Pollet, E., & Avérous, L. (2009). Nano-biocomposites: Biodegradable polyester/nanoclay systems. *Progress in Polymer Science, 34*(2), 125-155.

Caner, C., Vergano, P. J., & Wiles, J. L. (1998). Chitosan Film Mechanical and Permeation Properties as Affected by Acid, Plasticizer, and Storage. *Journal of Food Science, 63*(6), 1049-1053.

Chivrac, F., Pollet, E., & Avérous, L. (2009). Progress in nano-biocomposites based on polysaccharides and nanoclays. *Materials Science and Engineering: R: Reports, 67*(1), 1-17.

553 Darder, M., Colilla, M., & Ruiz-Hitzky, E. (2003). Biopolymer−Clay Nanocomposites Based
554 on Chitosan Intercalated in Montmorillonite. *Chemistry of Materials, 15*(20), 3774-3780.
555 Depan, D., Kumar, A. P., & Singh, R. P. (2006). Preparation and characterization of novel
556 hybrid of chitosan-g-lactic acid and montmorillonite. *Journal of Biomedical Materials*
557 *Research Part A, 78A*(2), 372-382.
558 Depan, D., Kumar, B., & Singh, R. P. (2008). Preparation and characterization of novel
559 hybrid of chitosan-g-PDMS and sodium montmorrilonite. *Journal of Biomedical*
560 *Materials Research Part B: Applied Biomaterials, 84B*(1), 184-190.
561 Dutta, P. K., Tripathi, S., Mehrotra, G. K., & Dutta, J. (2009). Perspectives for chitosan based
562 antimicrobial films in food applications. *Food Chemistry, 114*(4), 1173-1182.
563 Epure, V., Griffon, M., Pollet, E., & Avérous, L. (2011). Structure and properties of glycerol-
564 plasticized chitosan obtained by mechanical kneading. *Carbohydrate Polymers, 83*(2),
565 947-952.
566 Funabashi, M., Ninomiya, F., & Kunioka, M. (2009). Biodegradability Evaluation of
567 Polymers by ISO 14855-2. *International Journal of Molecular Sciences, 10*(8), 3635-
568 3654.
569 Guo, Z., Chen, R., Xing, R., Liu, S., Yu, H., Wang, P., Li, C., & Li, P. (2006). Novel
570 derivatives of chitosan and their antifungal activities in vitro. *Carbohydrate Research,*
571 *341*(3), 351-354.
572 Hosokawa, J., Nishiyama, M., Yoshihara, K., & Kubo, T. (1990). Biodegradable film derived
573 from chitosan and homogenized cellulose. *Industrial & Engineering Chemistry Research,*
574 *29*(5), 800-805.
575 Kabara, J. J., Conley, A. J., & Truant, J. P. (1972). Relationship of Chemical Structure and
576 Antimicrobial Activity of Alkyl Amides and Amines. *Antimicrobial Agents and*
577 *Chemotherapy, 2*(6), 492-498.

578 Kaushik, A., Khan, R., Solanki, P. R., Pandey, P., Alam, J., Ahmad, S., & Malhotra, B. D.
579 (2008). Iron oxide nanoparticles–chitosan composite based glucose biosensor. *Biosensors*
580 *and Bioelectronics, 24*(4), 676-683.
581 Kean, T., & Thanou, M. (2010). Biodegradation, biodistribution and toxicity of chitosan.
582 *Advanced Drug Delivery Reviews, 62*(1), 3-11.
583 Khan, R., Kaushik, A., Solanki, P. R., Ansari, A. A., Pandey, M. K., & Malhotra, B. D.
584 (2008). Zinc oxide nanoparticles-chitosan composite film for cholesterol biosensor.
585 *Analytica Chimica Acta, 616*(2), 207-213.
586 Kittur, F. S., Vishu Kumar, A. B., & Tharanathan, R. N. (2003). Low molecular weight
587 chitosans—preparation by depolymerization with Aspergillus niger pectinase, and
588 characterization. *Carbohydrate Research, 338*(12), 1283-1290.
589 Lau, C., Cooney, M. J., & Atanassov, P. (2008). Conductive Macroporous Composite
590 Chitosan−Carbon Nanotube Scaffolds. *Langmuir, 24*(13), 7004-7010.
591 Li, M., Liu, P., Zou, W., Yu, L., Xie, F., Pu, H., Liu, H., & Chen, L. (2011). Extrusion
592 processing and characterization of edible starch films with different amylose contents.
593 *Journal of Food Engineering, 106*(1), 95-101.
594 Li, Y., Wu, K., & Zhitomirsky, I. (2010). Electrodeposition of composite zinc oxide–chitosan
595 films. *Colloids and Surfaces A: Physicochemical and Engineering Aspects, 356*(1–3), 63-
596 70.
597 Liu, H., Xie, F., Yu, L., Chen, L., & Li, L. (2009). Thermal processing of starch-based
598 polymers. *Progress in Polymer Science, 34*(12), 1348-1368.
599 Pavlidou, S., & Papaspyrides, C. D. (2008). A review on polymer–layered silicate
600 nanocomposites. *Progress in Polymer Science, 33*(12), 1119-1198.

Quijada-Garrido, I., Laterza, B., Mazón-Arechederra, J. M., & Barrales-Rienda, J. M. (2006). Characteristic Features of Chitosan/Glycerol Blends Dynamics. *Macromolecular Chemistry and Physics, 207*(19), 1742-1751.

Quijada-Garrido, I., Iglesias-González, V., Mazón-Arechederra, J. M., & Barrales-Rienda, J. M. (2007). The role played by the interactions of small molecules with chitosan and their transition temperatures. Glass-forming liquids: 1,2,3-Propantriol (glycerol). *Carbohydrate Polymers, 68*(1), 173-186.

Rinaudo, M. (2006). Chitin and chitosan: Properties and applications. *Progress in Polymer Science, 31*(7), 603-632.

Sinha Ray, S., Okamoto, K., & Okamoto, M. (2003). Structure−property relationship in biodegradable poly(butylene succinate)/layered silicate nanocomposites. *Macromolecules, 36*(7), 2355-2367.

Sinha Ray, S., & Okamoto, M. (2003). Polymer/layered silicate nanocomposites: a review from preparation to processing. *Progress in Polymer Science, 28*(11), 1539-1641.

Thein-Han, W. W., & Misra, R. D. K. (2009a). Biomimetic chitosan–nanohydroxyapatite composite scaffolds for bone tissue engineering. *Acta Biomaterialia, 5*(4), 1182-1197.

Thein-Han, W. W., & Misra, R. D. K. (2009b). Three-dimensional Chitosan-nanohydroxyapatite Composite Scaffolds for Bone Tissue Engineering. *JOM, 61*(9), 41-44.

Tikhonov, V. E., Stepnova, E. A., Babak, V. G., Yamskov, I. A., Palma-Guerrero, J., Jansson, H.-B., Lopez-Llorca, L. V., Salinas, J., Gerasimenko, D. V., Avdienko, I. D., & Varlamov, V. P. (2006). Bactericidal and antifungal activities of a low molecular weight chitosan and its N-/2(3)-(dodec-2-enyl)succinoyl/-derivatives. *Carbohydrate Polymers, 64*(1), 66-72.

Wang, S.-F., Shen, L., Zhang, W.-D., & Tong, Y.-J. (2005a). Preparation and Mechanical Properties of Chitosan/Carbon Nanotubes Composites. *Biomacromolecules, 6*(6), 3067-3072.

Wang, S. F., Shen, L., Tong, Y. J., Chen, L., Phang, I. Y., Lim, P. Q., & Liu, T. X. (2005b). Biopolymer chitosan/montmorillonite nanocomposites: Preparation and characterization. *Polymer Degradation and Stability, 90*(1), 123-131.

Way, C., Wu, D. Y., Dean, K., & Palombo, E. (2010). Design considerations for high-temperature respirometric biodegradation of polymers in compost. *Polymer Testing, 29*(1), 147-157.

Xie, F., Halley, P. J., & Avérous, L. (2012). Rheology to understand and optimize processibility, structures and properties of starch polymeric materials. *Progress in Polymer Science, 37*(4), 595-623.

Xu, J., McCarthy, S. P., Gross, R. A., & Kaplan, D. L. (1996). Chitosan Film Acylation and Effects on Biodegradability. *Macromolecules, 29*(10), 3436-3440.

Yu, L., Dean, K., & Li, L. (2006). Polymer blends and composites from renewable resources. *Progress in Polymer Science, 31*(6), 576-602.